Published in final edited form as:
Phys Med Biol. 2012 January 21; 57(2): 375–393. doi:10.1088/0031-9155/57/2/375.

Investigation of dynamic SPECT measurements of the arterial input function in human subjects using simulation, phantom and human studies

Celeste D Winant[1,5], **Carina Mari Aparici**[1], **Yuval R Zelnik**[2], **Bryan W Reutter**[3], **Arkadiusz Sitek**[4], **Stephen L Bacharach**[1], and **Grant T Gullberg**[1,3,6]

[1]UCSF Physics Research Laboratory, Department of Radiology, University of California San Francisco, 185 Berry St, Suite 350, PO Box 0946, San Francisco, CA 94107, USA

[2]Edmond J Safra Campus, Hebrew University, Jerusalem 91904, Israel

[3]Lawrence Berkeley National Laboratory, One Cyclotron Road, Berkeley, CA 94720, USA

[4]Department of Radiology, Brigham and Women's Hospital and Harvard Medical School, Boston, MA 02115, USA

Abstract

Computer simulations, a phantom study and a human study were performed to determine whether a slowly rotating single-photon computed emission tomography (SPECT) system could provide accurate arterial input functions for quantification of myocardial perfusion imaging using kinetic models. The errors induced by data inconsistency associated with imaging with slow camera rotation during tracer injection were evaluated with an approach called SPECT/P (dynamic SPECT from positron emission tomography (PET)) and SPECT/D (dynamic SPECT from database of SPECT phantom projections). SPECT/P simulated SPECT-like dynamic projections using reprojections of reconstructed dynamic ^{94}Tc-methoxyisobutylisonitrile (^{94}Tc-MIBI) PET images acquired in three human subjects (1 min infusion). This approach was used to evaluate the accuracy of estimating myocardial wash-in rate parameters K_1 for rotation speeds providing 180° of projection data every 27 or 54 s. Blood input and myocardium tissue time-activity curves (TACs) were estimated using spatiotemporal splines. These were fit to a one-compartment perfusion model to obtain wash-in rate parameters K_1. For the second method (SPECT/D), an anthropomorphic cardiac torso phantom was used to create real SPECT dynamic projection data of a tracer distribution derived from ^{94}Tc-MIBI PET scans in the blood pool, myocardium, liver and background. This method introduced attenuation, collimation and scatter into the modeling of dynamic SPECT projections. Both approaches were used to evaluate the accuracy of estimating myocardial wash-in parameters for rotation speeds providing 180° of projection data every 27 and 54 s. Dynamic cardiac SPECT was also performed in a human subject at rest using a hybrid SPECT/CT scanner. Dynamic measurements of ^{99m}Tc-tetrofosmin in the myocardium were obtained using an infusion time of 2 min. Blood input, myocardium tissue and liver TACs were estimated using the same spatiotemporal splines. The spatiotemporal maximum-likelihood expectation-maximization (4D ML-EM) reconstructions gave more accurate reconstructions than did standard frame-by-frame static 3D ML-EM reconstructions. The SPECT/P results showed that 4D ML-EM reconstruction gave higher and more accurate estimates of K_1 than did 3D ML-EM, yielding anywhere from a 44% underestimation to 24% overestimation for the three patients. The SPECT/D results showed that 4D ML-EM reconstruction gave an overestimation of 28% and 3D

[6]Author to whom any corresspondence should be addressed. gtgullberg@lbl.gov.
[5]Present address: Department of Demography, UC Berkeley, 2232 Piedmont Avenue, Berkeley, CA 94720-2120, USA.

ML-EM gave an underestimation of 1% for K_1. For the patient study the 4D ML-EM reconstruction provided continuous images as a function of time of the concentration in both ventricular cavities and myocardium during the 2 min infusion. It is demonstrated that a 2 min infusion with a two-headed SPECT system rotating 180° every 54 s can produce measurements of blood pool and myocardial TACs, though the SPECT simulation studies showed that one must sample at least every 30 s to capture a 1 min infusion input function.

1. Introduction

Measurement of the arterial input function (AIF) is essential to deriving quantitative estimates of regional myocardial blood flow using kinetic models. Accurate measurement of the AIF with dynamic single-photon computed emission tomography (SPECT) is challenging because the tracer distribution changes as the scanner rotates, yielding inconsistent projections. A positron emission tomography (PET) camera is able to image the radiotracer distribution simultaneously at all angles at every time point, and accurate measurements of the AIF with PET have been made with a wide range of radiotracers (Klein *et al* 2010, Iida *et al* 1992, Yoshida *et al* 1996). While some of the newest SPECT cameras can image many projections simultaneously (Patton *et al* 2007), most SPECT cameras can only measure one to three projections at a time. To obtain the remaining angular views, the camera must rotate around the patient. During this rotation, the radiotracer distribution within the patient can vary, especially during measurement of an AIF. Most standard reconstruction algorithms assume a temporally consistent set of projection data. The reconstruction of inconsistent data due to temporal variations in the distribution of the radiotracer can produce artifacts and errors in quantification.

Modifications can be made to the scanning protocols with conventional cameras that can shorten the SPECT camera rotation time. The cameras can acquire data continuously while rotating (as opposed to ‘step and shoot’), as well as sweep through the entire set of projection angles multiple times during the period of fastest kinetics in the radiotracer distribution (Farncombe *et al* 1999, Celler *et al* 2001, Sitek *et al* 2001, Feng *et al* 2006, Gullberg *et al* 2010). Also, the implementation of spatiotemporal reconstruction methods that use spatial and temporal basis functions to reconstruct the projection data can partially compensate for the relatively slow rotation speed of conventional SPECT cameras, thus reducing the bias due to inconsistent projection measurements (Reutter *et al* 2000, 2002, 2004, 2005).

In this paper we investigated how accurately an existing conventional SPECT camera (Philips Precedence™ (Cleveland, OH) dual-headed hybrid SPECT and x-ray computed tomography (SPECT/CT) camera) can measure the AIF. To perform these investigations, we used ^{94}Tc-methoxyisobutylisonitrile (^{94}Tc-MIBI) dynamic PET patient data as a referenced standard against which to compare the equivalent SPECT results. The equivalent SPECT data were simulated by reprojecting the reconstructed dynamic PET image sequence into SPECT projections that would have been obtained from the Philips SPECT camera (SPECT/P). To our knowledge this is the first use of PET data to simulate SPECT data, which we previously reported in an abstract (Winant *et al* 2009a) and a paper in a proceedings (Winant *et al* 2009b). In addition, we investigated the potential artifacts and errors resulting from inconsistent SPECT projections by using a database of real dynamic SPECT projection data (Sitek *et al* 2006) from a physical phantom. This phantom-based method correctly accounted for the photon statistics, attenuation, scatter and collimator blurring of SPECT data, making it complementary to the PET-based method described above. We compared the PET reconstructed patient data to reconstructions of the SPECT/P data and of the SPECT/D data using both conventional frame-by-frame static SPECT reconstruction methods (3D

reconstruction, SPECT/P-3D, and SPECT/D-3D) and spatiotemporal reconstruction methods (SPECT/P-4D and SPECT/D-4D). We compared the images, the time–activity curves (TACs), and parameters from single-compartment kinetic analysis from the PET patient data to those from the equivalent simulated SPECT data. We also present the results of estimating the AIF from a SPECT patient study. This study provided the impetus to perform simulation studies to verify the results.

2. Methods

2.1. SPECT from ^{94}Tc-MIBI PET

Previously acquired ^{94}Tc-MIBI PET scans of three subjects (patients 1, 2, and 3) were used as a referenced standard against which to compare equivalent SPECT data. These subjects were studied to monitor solid, non-cardiac tumors. They were not evaluated for cardiac disease. Each subject was positioned so that the heart was in the field of view of the PET scanner (GE Advance, GE Healthcare, Waukesha, WI). Approximately 259 MBq (7 mCi) of ^{94}Tc-MIBI was infused over 60 s using a constant speed pump (Harvard Apparatus 975). PET data were acquired dynamically for 85 min (12 frames of 15 s, 12 of 30 s, 12 of 60 s, and 16 of 240 s). Reconstruction (ordered-subset expectation maximization (OS-EM), 28 subsets, four iterations) yielded 37 transaxial slices per time frame (pixels of 2 mm × 2 mm in plane, 4.25 mm slice separation). Attenuation correction was performed with use of transmission data acquired with a rotating ^{68}Ge rod source. TACs were created from volumes of interest (VOIs) in the left ventricular myocardium, the left ventricular/left atrial (LV/LA) blood pool and the liver.

The PET data were used to simulate a SPECT acquisition with a two-headed Philips Precedence™ camera. It was able to rotate 90° in 54 s, with the detectors in ‘L’ mode (90° separation), using a continuous rotation, and then instantaneously reverse direction for the next rotation. Projection data were binned into angular bins with 5° increments, yielding 18 angular bins per head acquired in time steps of 3 s/bin. Each 54 s rotation yielded 36 angular projections that provided views spanning a range of 180° from right anterior oblique to left posterior oblique. Each 180° data set could then be reconstructed into a single set of transaxial images, each with 128 × 128 voxels of dimension 3.19 mm × 3.19 mm × 3.19 mm.

A time sequence of images reconstructed from the dynamic ^{94}Tc-MIBI PET data was used to create the equivalent SPECT/P projection data. The PET camera acquired temporally consistent projection data for every time frame at all angles. The PET images were first resampled to the same voxel size as used in the clinical SPECT camera, and were temporally interpolated to match the 3 s timing of the individual frames of the SPECT acquisition. Each image in this sequence was then reprojected (including collimator blurring and attenuation calculated from transmission data for the PET study rescaled to an attenuation coefficient for 140 keV) at the appropriate angle for each head to produce the SPECT/P data set. We synthesized the 36 projection data frames that would have been acquired by the two heads of our SPECT camera during each 54 s rotation. This procedure was repeated for each of the eight sequential rotations.

Our SPECT camera was limited to a maximum angular rotation speed of 90°/54 s. However we explored the effect of faster camera rotation speeds by using different temporal resamplings of the dynamic PET images, keeping 36 angular views per rotation with the same spatial sampling and pixel size. We created SPECT/P data for 8 rotations of 54 s and 16 rotations of 27 s, each yielding a total imaging time of 432 s.

Attenuation and geometric point response were modeled into the SPECT/P data using a ray-driven projector with line length weighting as described in Zeng *et al* (1991). Attenuation was determined using the ^{68}Ge transmission images acquired during the PET study. The linear attenuation coefficients were converted from 511 to 140 keV. Collimation-induced blurring was computed analytically using the geometric parameters of the Philips Precedence™ low-energy high-resolution (LEHR) collimator. Realistic Poisson noise was incorporated into the SPECT/P projections. The magnitude of the noise was taken from 54 s per rotation SPECT dynamic patient data, measured with the Philips Precedence™ SPECT/CT camera using the described acquisition parameters. The variances of the projection data for the 27 s per rotation SPECT/P data were taken to be one-half those of the 54 s per rotation SPECT/P data. In summary, attenuation, collimator-induced blurring, and realistic noise were modeled into the projection data. Scatter was not modeled into the projection data.

The SPECT/P projections were reconstructed with two different maximum-likelihood expectation maximization (ML-EM) algorithms (50 iterations). For the first, a standard static ML-EM reconstruction, referred to as 3D reconstruction, was used for each rotation. Each rotation produced a reconstructed image for a single time frame. For the second, we applied a spatiotemporal reconstruction method, referred to as 4D reconstruction. This method assumes that the activity in each voxel varies smoothly as a function of time and can be described by a piecewise quadratic TAC that is obtained as a linear combination of pre-defined mathematical 'basis' functions. These piecewise quadratic curves can represent a variety of TACs, such as the blood input functions and tissue uptake curves obtained in real patient data. The temporal basis functions were a set of five overlapping quadratic B-spline functions defined on a time grid that provided nonuniform sampling intervals of 0–12, 12–36, 36–72, 72–120, 120–216, and 216–432 s, analogous to the dynamic PET time frames. The time-varying activity associated with each of the B-spline functions was incorporated into the forward-projection model for counts detected from each voxel at each angular position of the SPECT detector heads, for each of the rotations. TACs for all voxels were then obtained by estimating amplitude coefficients for the B-spline functions directly from the dynamic SPECT projection data. Because the five B-spline functions overlapped each other in time (to provide continuous TACs), data from all rotations had to be processed simultaneously so that the five coefficients for each voxel could be jointly estimated. The 4D reconstruction method is described in more detail in Reutter *et al* (2000, 2005).

VOIs from the combined LV/LA blood pool, from the left ventricular myocardium and from the liver were identified on early-summed and late-summed PET dynamic images. TACs were created by overlaying these VOIs on the dynamic PET images and on both the dynamic 3D ML-EM- and 4D ML-EM-reconstructed SPECT/P images.

We gauged the accuracy of the dynamic SPECT TACs from inconsistent projection data with two measures. First, we compared compartmental TACs from the gold-standard PET images to those from the SPECT/P images. Second, we compared the kinetic parameters derived from the PET TACs with those from the reconstructed SPECT/P TACs, using the nonlinear single-compartment model (Coxson *et al* 1992, Iida and Eberl 1998, Lortie *et al* 2007, Iida *et al* 2008) which is parameterized by uptake (K_1), wash-out (k_2) and vascular spillover into the tissue (f_v). The single-compartment model was taken to be

$$Q_M(t)=(1-f_v)K_1\int_0^t Q_B(\tau)\mathrm{e}^{-k_2(t-\tau)}\mathrm{d}\tau+f_vQ_B(t), \quad (1)$$

where $Q_M(t)$ was the activity of the radionuclide in the myocardium (Bq/cc), $Q_B(t)$ was the activity in the AIF (Bq/cc), K_1 was the uptake parameter, k_2 was the wash-out parameter

(both measured in units of inverse minutes (min^{-1})) and f_v was the blood fraction in the myocardium.

2.2. Statistical analysis

Pearson correlation coefficients were calculated to quantitatively compare SPECT/P 3D ML-EM versus 4D ML-EM images for patient 1, using PET images as the referenced standard. This was done through pixel-by-pixel comparisons between the cardiac portions (a single transaxial slice) of the PET image and the respective corresponding slice in the SPECT/P 3D and the SPECT/P 4D images. The low SNR required that several pixels be used to achieve a statistically reliable correlation. It was necessary to ensure that the pixels were independent of one another (i.e. were not themselves spatially correlated). The pixels were determined to be independent of one another if they were >2 FWHM (2.6 cm) apart. The significance of the differences between correlation coefficients for the 3D ML-EM and 4D ML-EM estimates were tested by calculating the standard normal *Z* statistic (Zar 1999).

Dunnett's test for multiple comparisons (Zar 1999) was used to compare the value of K_1 from each SPECT analysis with the PET reference standard. Dunnett's test is specifically designed for this type of multiple comparison analysis because with multiple comparisons, the probability of obtaining a statistically significant difference simply by chance increases and the critical *Q* value is effectively reduced. Appropriate tables for $\alpha = 0.05$ and $\alpha = 0.01$ were employed.

A two-way analysis of variance (ANOVA) between groups was also performed to determine the between-method (SPECT/P 27 s or 54 s rotation; 3D- or 4D ML-EM analysis) and the between-patient (three in total) proportions to the variance in the estimated K_1 parameters. The analysis assumed the following model:

$$Y_{ij}=\mu+P_i+M_j, \tag{2}$$

where Y_{ij} was the bias between the SPECT/P method and the PET method, μ was the true bias that was being estimated by the model, P_i was the patient random factor and M_j was the SPECT/P-method fixed factor. Both error and interaction terms were left out of the analysis, given the lack of replication of data in each cell. It was assumed that both factors (methods and patients) were truly random.

2.3. Dynamic SPECT database study

We also created dynamic SPECT data (referred to as SPECT/D) using a database of SPECT measurements of an anthropomorphic torso phantom (Jaszczak cardiac torso phantom, Data Spectrum Corporation, Hillsborough, NC). The details of generating the database have been described elsewhere (Sitek *et al* 2006).

The phantom data were acquired with a GE Millennium™ VG3 camera with Hawkeye™ attenuation correction (GE Healthcare, Haifa, Israel), using a LEHR collimator. The left ventricle, myocardium, liver and background were respectively filled with known concentrations of ^{99m}Tc-pertechnetate. A series of projection images were made of the activity in each compartment, over a range of 360° (120 angles). For each compartment, 300 projections of duration 0.5 s were measured at each angle. CT scans of the phantom were part of the database and were used for attenuation correction.

We used the previously described blood pool, myocardial and liver TACs from ^{94}Tc-MIBI patient 1 as input radiotracer distributions to the database. The background activity was assumed to be 10% of the liver activity. The PET input functions were scaled by a multiplicative factor to generate similar statistics as in the patient study, assuming a SPECT

radiotracer injection dose of 925 MBq (25 mCi). The acquisition was based on the 54 s rotation and acquisition parameters used in the SPECT/P study, although the database angular sampling had to be used (60 angles over 180°, each projection separated by 3°). The database was then used to produce the projections at each angle according to the assumed number of angles, projection-duration and input activity. The collection of SPECT/D projections was then reconstructed with the same 3D ML-EM and 4D ML-EM reconstruction methods described previously.

VOIs in the left ventricle, myocardium, liver and background were drawn on the Jaszczak phantom CT images. TACs for the blood pool, myocardium and liver were generated from the mean activity measured in these regions, as superimposed on the SPECT/D images. The TACs were scaled by the left ventricle, myocardium and liver mixing coefficients to correct for residual partial volume, attenuation and scatter artifacts in the images. The TACs, $T_i(t)$ {*i: b* = blood, *m* = myocardium, *l* = liver}, were corrected through multiplication by the inverse of the matrix *M*:

$$\tilde{T}_i(t)=\mathrm{inv}(M)_{ij}T_j(t), \tag{3}$$

where

$$M=\begin{bmatrix} m_{bb} & m_{bm} & m_{bl} \\ m_{mb} & m_{mm} & m_{ml} \\ m_{lb} & m_{lm} & m_{ll} \end{bmatrix}=\begin{bmatrix} 0.4020 & 0.0690 & 0.0100 \\ 0.0310 & 0.2190 & 0 \\ 0.007 & 0.007 & 0.3220 \end{bmatrix}, \tag{4}$$

$m_{i\,j}$ were the mixing coefficients between compartments *i* and *j* and $\tilde{T}_i(t)$ was the corrected TAC for the compartment *i*. These coefficients were measured from three sets of separately-generated temporally consistent SPECT/D projections of the phantom with unit input in the three respective compartments of interest. Note that these correction coefficients were specific to the regions of interest used for this validation. This corrective procedure has been validated elsewhere (Tang *et al* 2001). Comparisons between the dynamic SPECT/D TACs and the PET TACs (taken as 'truth') were made as described previously for the case of the SPECT/P data.

2.4. Dynamic SPECT patient study

One patient was imaged at rest with a Philips Precedence™ SPECT/CT dual-headed scanner. An injection of 636 MBq (17.2 mCi) of ^{99m}Tc-tetrofosmin was delivered in a constant 2 min infusion using a Harvard Apparatus Model 975 pump while the patient was lying supine. Imaging began at the start of infusion, using a series of eight back-to-back 180° continuous-mode acquisitions (54 s for each circular rotation), with the heads at 90°, at a radial distance of 30 cm away from the center of the rotation; circular (versus body contour) achieved fastest camera rotation speeds. A set of 36 projections (128 × 128 pixels of dimension 3.19 mm × 3.19 mm) was acquired during each rotation, yielding a total acquisition time of 432 s. The dynamic projections were reconstructed with the same 3D and 4D methods described above for the SPECT/P. The SPECT and CT images were co-registered with the Philips JetStream™ Workstation and Astonish™ OS-EM-based software.

3. Results

3.1. SPECT from ^{94}Tc-MIBI PET

Images from ^{94}Tc-MIBI PET and from the 54 s per rotation ^{99m}Tc-MIBI SPECT/P data for patient 1 are shown in figure 1. The top row shows images obtained during the first 60 s of imaging (during the period of radiotracer injection). The bottom row shows summed images

from late times (270–420 s). The PET images are shown in the first two columns, both with no additional filtering (left column 1) and with 14 mm Gaussian post reconstruction filtering (column 2), matching the measured point-spread blurring of the center of the image for data acquired with the Philips Precedence™ camera, given a detector orbit radius of 30 cm. This filtering makes the images easier to compare to the lower resolution SPECT/P data. The 3D ML-EM reconstructed SPECT/P images are shown in column 3, while the 4D reconstructed images are shown in column 4.

All SPECT/P images have evidence of artifacts, especially at early times. The activity in the blood pool at early times in the 3D ML-EM image is inhomogeneous. Low-level spiral streak-artifacts emanate from regions of high radiotracer activity in the early 4D ML-EM images. The correlation coefficients for the early-time SPECT/P 3D ML-EM and SPECT/P 4D ML-EM images compared to the PET image for 64 independent samples were 0.84 ($p < 0.0001$) and 0.94 ($p < 0.0001$), respectively. In addition to the two correlation coefficients being highly statistically significant individually, the differences between the two estimates were also highly statistically significant employing the standard normal Z statistic. The results were $Z = 2.87$ with $p = 0.004$.

Figure 2 compares the PET TACs (solid lines) with the corresponding SPECT/P TACs for blood pool, myocardium and liver for patient 1. For SPECT/P reconstructions both standard rotation-by-rotation 3D reconstruction (stars) and 4D reconstruction (dashed lines) are shown along with the input PET curves (solid lines). The 27 s per rotation SPECT/P acquisition is shown in figure 2(A), and the 54 s per rotation is shown in figure 2(B). There is good visual agreement between SPECT/P and PET TACs, although at early times, the 4D reconstructed SPECT/P blood pool TAC seems to underestimate the true PET values. At later times (>100 s), for both 3D and 4D reconstructions, the SPECT/P myocardial TACs underestimate the true PET data. As expected, there appears to be more noise in the 3D than the 4D reconstructed SPECT/P data because the 4D reconstruction of TACs involves fitting projection data to a few temporal spline basis functions yielding smooth TACs.

The fractional differences (i.e. residuals) between the TACs from PET and standard 3D ML-EM reconstruction of SPECT/P data for both blood and myocardial tissue, averaged over all three PET patients, are shown in figure 3. The difference curve for each VOI and patient was first normalized by the average of the corresponding gold-standard PET curve.

The mean and standard deviation of these residuals for the 27 s per rotation data, averaged over 420 s of imaging, were respectively +5.8% ± 19.6% for the blood curves and −13.4% ± 6.6% for the myocardium curves. The mean and standard deviation of these residuals for the 54 s per rotation data, averaged over 420 s of imaging, were respectively +9.1% ± 22.0% for the blood curves and −11.2% ± 8.3% for the myocardium curves. For both rotation speeds, we see systematic underestimation of the SPECT/P myocardium curves and a systematic overestimation of the input curves for later times ($t > 100$ s.)

The SPECT/P AIF and myocardial TACs were used to compute kinetic parameters from a single-compartment model. Table 1 compares these kinetic parameters, along with the 1σ (unweighted) fit errors, to the same parameters derived from the PET TACs.

For all patients and rotation speeds, 4D ML-EM reconstruction always gave higher estimates of the single-compartment uptake parameter, K_1, than did 3D ML-EM reconstruction. Except for SPECT/P 54 s rotation data for patient 1, 4D ML-EM also gave more accurate results for K_1 than did 3D ML-EM. For patients 1 and 3, the SPECT/P uptake parameters were (except for patient 1, 4D ML-EM) underestimated by as much as 19% for the 27 s rotation data, and were (except for patient 3, 3D ML-EM) overestimated by as much as 23% for the 54 s rotation data. The uptake parameter K_1 for SPECT/P patient 2 had the largest

bias (underestimated by 32% for 4D ML-EM and 38% for 3D ML-EM averaged over the two camera rotation speeds). Table 1 indicates the biases that were statistically significant at the 0.05 and 0.01 level employing Dunnett's test.

From a two-way (method/patient) ANOVA analysis, the results also showed that there were statistically significant differences between methods ($p = 0.012$) and between patients ($p = 0.001$). A total variance of 0.0059 was computed for the 12 estimated biases shown in table 1. The between-patient proportion of total variance was 69%. The between-method proportion of total variance was 23%. The random error proportion of total variance was 8%. This shows that there was more variation between the three patients than there was between the four methods.

3.2. Dynamic SPECT database study

The 4D ML-EM and 3D ML-EM reconstructions of SPECT/D data for early- and late-time images are shown in figure 4. The early blood pool 3D ML-EM images have artifacts at the anatomical boundary of the torso, and early blood pool 4D ML-EM images have artifacts near the cardiac insert. The late images appear to be similar.

The input functions derived from PET ^{94}Tc-MIBI TACs, which were used to parameterize the data selection from the database, are compared in figure 5(A) with the TACs estimated from the dynamic image reconstructions for blood pool, myocardium and liver. For SPECT/D reconstructions, both standard 3D reconstruction (stars) and 4D reconstruction (dashed lines) TACs are shown in comparison with the input PET TACs (solid lines).

Residual differences between the PET and 3D ML-EM SPECT/D TACs for both blood and myocardium tissue TACs are shown in figure 5(B). The means and standard deviations of the difference curves were $-14.1\% \pm 9.2\%$ and $-0.7\% \pm 5.5\%$, respectively, for the residual blood pool and myocardial tissue curves. The SPECT/D data gave a systematic underestimation of the blood pool curve at all times, but a very close estimate of the myocardium curve.

We obtained uptake parameter (K_1) estimates of 0.542 ± 0.005 and 0.420 ± 0.042 min^{-1}, respectively, from nonlinear fitting of a single-compartment model with uptake and wash-out, for the 4D ML-EM and 3D ML-EM reconstruction of SPECT/D data of 54 s per rotation. These estimates are, respectively, 28% over and 1% under the estimate for the gold-standard PET uptake parameter for patient 1 (table 1).

3.3. Dynamic SPECT patient study

The 1 min infusion PET and SPECT/P simulation studies led us to discover that one must sample at least every 30 s to capture a 1 min^{-1} infusion input function. However, the SPECT camera could only produce one sample every minute (max rotation speed of 1 rotation min^{-1}). Therefore, the infusion time was lengthened by a factor of 2 (to 2 min). Early- and late-time images from the dynamic patient study, reconstructed with the 4D ML-EM algorithm, are shown in figure 6. We show the images from two different times: from 2 min after the beginning of the 2 min infusion (top row of figure 6) and from 6–7.2 min after the beginning of the infusion (bottom row of figure 6). The activity is concentrated in both ventricular cavities at early times and in the myocardium and liver at later times. At later times (after 120 s of imaging), the mean activity in the region of the left ventricular myocardium is 1 count per pixel per 3 s projection.

We compare TACs from both the 3D ML-EM and 4D ML-EM reconstructions in figure 7. The selected VOIs for both reconstructions were defined by thresholding the 4D reconstructed images shown in figure 6 (left ventricle from the early image, myocardium

and liver from the late image), within anatomical boundaries determined from the registered CT image.

4. Discussion

In this paper we developed a methodology for the processing of dynamic data acquired from a commercial slowly rotating dual-headed SPECT scanner. Accurate measurement of the AIF with dynamic SPECT has been limited by bias introduced from imaging a rapidly changing radiotracer distribution with a slowly rotating scanner. Improved results can be obtained with standard 3D reconstruction of tomographic acquisitions of 1 rotation per min if the infusion of the tracer is lengthened to match the timing resolution of the SPECT camera. A data processing algorithm was developed to fit the acquired tomographic data of the concentration activity changing from projection to projection to spatiotemporal splines. Using spatiotemporal splines, 4D processing provided even more accurate measures of the AIF. To investigate the accuracy of 3D and 4D processing of dynamic SPECT data compared with PET, we used the SPECT/P and the SPECT/D methodologies to compare the quantitative accuracy in estimating kinetic rate parameters. The SPECT/P methodology simulated dynamic SPECT data using human PET data dynamically acquired with the same radiopharmaceutical used in clinical cardiac SPECT studies. The SPECT/D methodology simulated dynamic SPECT data using data from a database of real SPECT projections of ^{99m}Tc in blood pool, myocardium, liver and background compartments of an anthropomorphic cardiac torso phantom. A human SPECT study with slow camera rotation using a 2 min infusion showed the potential of the technique to estimate rates of wash-in and wash-out of ^{99m}Tc-tetrofosmin in the heart. The technique has potential to provide coronary flow reserve (CFR), which has been shown to provide incremental prognostic information, particularly in patients with normal perfusion (Daniele *et al* 2011, Murthy *et al* 2011).

The SPECT/P and the SPECT/D methodologies involved modeling of the Philips Precedence™ SPECT/CT camera, which was investigated by performing dynamic SPECT clinical imaging on human subjects. The patient study allowed us to demonstrate the feasibility of performing the described dynamic acquisition (imaging a slow, controlled infusion with eight 54 s back-to-back continuous rotations) with an existing commercial scanner. We were also able to characterize the noise in the short dynamic projection-measurements, which we used in our SPECT/P and SPECT/D validations. In order to achieve the desired scan speeds, the camera had to be rotated in a circular (versus body contour) orbit, yielding a tradeoff in resolution (14 mm FWHM blurring, on average). Dynamic measurements of ^{99m}Tc-tetrofosmin in the myocardium were obtained using an infusion time of 2 min. We explored shorter infusion times of 1 min (in hopes of obtaining better frame-to-frame statistics) with the two complementary methodologies. The SPECT/P data used true physiological distributions of a myocardial perfusion imaging (MPI) tracer in human subjects. The SPECT/D data provided real attenuation, scatter, collimator-induced blurring and SPECT-like statistics in the projections.

The 4D ML-EM SPECT/P reconstructions show better agreement with the PET images at early times than do the 3D ML-EM reconstructions. At early times, the rapidly changing evolution of the tracer distribution led to inconsistent projections, which made 3D ML-EM less accurate. It has been shown that attenuation can amplify the inaccuracy in solving the inverse of this underdetermined system of projection equations, even if the attenuation is modeled in the system matrix (Humphries *et al* 2011). At later times, when the radiotracer concentration stabilized, inconsistent projections were less of an issue, and images from both reconstruction methods were essentially identical. Both 3D and 4D ML-EM early SPECT/D images had artifacts. The artifacts in the 4D ML-EM images were closer to the cardiac insert, which could lead to greater error in VOI-based kinetic analysis.

The SPECT/P images had poorer resolution than the original PET images, despite correction for collimator response in both the 3D and 4D ML-EM reconstruction methods. This could be explained by the limited number of angles (36 per rotation), the distance of the camera from the center of rotation (30 cm) and the number of iterations per reconstruction (50).

All 4D ML-EM TACs presented in this paper (figures 2 and 7) are point-wise smoothed by the chosen temporal basis functions. Assessment of the agreement between SPECT/P AIFs and PET AIFs at early times is influenced by choice of sampling. Underestimation of the SPECT/P myocardium TAC and overestimation of the SPECT/P AIF at later times, as seen in figures 2 and 3, can be explained by the greater partial volume effects in SPECT compared to PET. We saw better agreement between the SPECT/P and PET liver curves, where partial volume errors are less.

In most cases, the estimate of the uptake parameter, K_1, from the nonlinear single-compartment model with uptake and wash-out, was also underestimated with SPECT/P. It is not possible to gauge with this small sample size of three patients whether 3D- or 4D ML-EM reconstruction leads to more accurate parameter estimation, especially given that patient variance dominated the overall variance in the bias. The one trend of note is that the estimate of the uptake parameter, K_1, from the single-compartment model with uptake and wash-out from the SPECT/P and SPECT/D 4D ML-EM reconstructed data, was systematically higher (although with less absolute bias except for one case) than the corresponding estimates from the 3D ML-EM reconstructed data.

We see similar trends with the dynamic SPECT/D data. The images show the expected concentration of radiotracer in the blood pool at early times, followed by accumulation in the myocardium, liver and background at later times. There is excellent agreement between the original PET and estimated 4D ML-EM SPECT/D myocardium tissue curves, whereas the SPECT/D AIF is underestimated compared to the PET AIF at all times. This trend differs from that seen with the SPECT/P TACs, possibly because there was no myocardial motion in the SPECT/D data, whereas such motion was present in the SPECT/P data. The estimates of the SPECT/D TACs also depend on the correct mixing coefficients, which were derived with independent database inputs.

As with the SPECT/P data, the 4D ML-EM SPECT/D estimate of the single-compartment model uptake parameter, K_1, was larger than the corresponding estimate from 3D ML-EM SPECT/D. With the single sample size, we cannot yet conclude the general trends in bias in estimating kinetic parameters from single-compartment models.

The SPECT/P and SPECT/D results demonstrate that dynamic SPECT can produce TACs of the blood pool and the myocardium which are quite close to the true values measured by PET, despite temporal inconsistencies in the projection data. The feasibility of true dynamic SPECT in the clinic requires a relatively slow injection of the imaged radiotracer. We estimated that the injection should be slower than the speed as the full camera rotation (longer than 1 min for the Philips Precedence™ SPECT/CT camera). Commercial infusion pumps allow for regulated, slow injections; however, care must be taken to not over-dilute the first-pass of the bolus through the cardiac field of view. A systematic study of injection speed versus camera rotation speed is needed to better address this question.

In previous work, several different input function shapes and sampling rates were studied for optimizing the precision and accuracy of kinetic rate parameters for dynamic cardiac SPECT (Ross *et al* 1997). These were analyzed for complete tomographic acquisitions of 10, 20 and 40 s, shorter than the 60 s acquisition of our SPECT camera. It was found that good statistics are more important than temporal sampling resolution when estimating fast kinetics. However, the analysis is difficult because of the many variables (infusion time, acquisition

timing, statistics of the injected dose, flow rate and extraction characteristics) in the acquisition of dynamic cardiac SPECT data, in addition to many parameters involved in optimizing the reconstruction methods. In this paper, our approach was to match, as accurately as possible, the infusion rate with the acquisition speed of the SPECT camera to obtain a timing resolution that could obtain the important characteristics of the input function and the temporal response of the heart. This was done to see if we could obtain information about kinetics even from standard 3D reconstruction without any 4D data analysis. The results have increased our interest to further validate the method in clinical studies comparing dynamic cardiac SPECT with slow rotation with dynamic cardiac PET using $^{13}NH_3$. The study has also encouraged us to examine the possibility of evaluating the method with dedicated cardiac SPECT cameras that would allow for the acquisition of consistent data for better quantification of cardiac perfusion.

Spatiotemporal splines were used to fit projection data of the radiotracer distribution which can change significantly in concentration from projection to projection. Zero-order spatial splines (voxels) and second-order temporal splines were used to fit the dynamically acquired tomographic data. Since the fits provide a continuous curve in time, one is able to provide an image of the heart and blood pool at any time during the infusion of the tracer as shown in figure 6. This involves a least-squares fit to the data in space and time and represents a very underdetermined problem because of the few samples for a very large number of unknowns. It is recognized that this may provide less than accurate TACs compared to the truth because the spatial temporal splines provide a smoothing of the dynamic TACs which tends to smooth out high frequency components. Accurately estimating the shape of the AIF is often critical for the estimation of the compartmental model parameters. Therefore, it is important to match the tracer infusion rate to the organ response and the sampling of the camera. In our case, the method may work fairly well because the source remains confined spatially during the time the tracer concentration is changing most rapidly from projection to projection. There is more work to be done to evaluate these many aspects of the physiology and the camera capabilities and to investigate the utilization of higher order spatial splines.

Currently, SPECT MPI is the most widely employed noninvasive method for the diagnosis and risk stratification of patients with known or suspected coronary artery disease (CAD) (Botvinick 2001, Beller 2009, Camici and Rimoldi 2009, Gould 2009, Hendel *et al* 2010). Cardiac MRI is making inroads into care of cardiac patients and play complementary roles in evaluation of patients with coronary disease. Cardiac MRI provides high-resolution images which enable the diagnosis of endocardial ischemia and late enhancement imaging that is prognostic for poor cardiac viability, and is showing progress in the application of dynamic MRI. However, not all patients can have an MRI scan, for example, patients with metal implants, patients who are claustrophobic, or patients who have ECG problems. From the standpoint of availability and economy of costs, the nuclear scintigraphic method (PET and SPECT) provides a convenient, noninvasive measure of myocardial perfusion and its hyperemic response to stress. Evaluation of flow differences before and after stress is the common basis of all stress testing for the diagnosis and risk stratification of CAD. The nuclear approach has the advantage of sensitivity and quantitation relative to other methods. The short decay times for isotopes used in PET allow for multiple scans making rest/stress studies easy to implement. However, PET requires either a cyclotron or an expensive generator which can make the procedure more expensive. SPECT is less expensive, readily available, does not require a cyclotron, and can perform dual isotope studies. This makes possible simultaneous perfusion and metabolic studies or simultaneous perfusion and innervation studies.

Adding dynamic capability to the widely available SPECT MPI method may permit quantitation of regional CFR (Gullberg *et al* 2001). Dynamic SPECT acquisitions, at rest

and during (pharmacologic) stress, could give three-dimensional CFR parametric images of resolution equal to that of the conventional static images by calculating the ratio of the wash-in at stress to the wash-in at rest. This would further enhance the utility of SPECT MPI, particularly in clinics where other modalities such as PET are not available. New dedicated cardiac SPECT scanners with CZT technology promise to yield more accurate CFR with clinically useful protocols that could provide dynamic rest/stress imaging in less than 15 min (Patton *et al* 2007). There are even some groups (Sugihara *et al* 2001, Daniele *et al* 2011, deKemp *et al* 2011) that have demonstrated the potential of using dynamic planar imaging with SPECT to obtain CFR measurements. It would be expected that dedicated cardiac systems would even be able to provide more accurate CFR measurements than these planar systems (Ben-Haim *et al* 2011).

5. Conclusion

Measurement of the AIF with SPECT has been thought to require ultra-fast camera rotations, due to the rapidly changing tracer distributions. However, we showed that with a 2 min tracer infusion and a 54 second rotation speed, a standard two-headed gamma camera can produce measurements of blood pool and myocardial TACs. These results held for both conventional 3D reconstructions of each time point, and for 4D reconstructions, although the latter may offer better temporal sampling. These findings are justification for performing further clinical validations, which if successful will allow SPECT to be used for many of the quantitative kinetic analyses now possible primarily with PET.

Acknowledgments

We thank Youngho Seo, Lingxiong Shao, and Xiyun Song for their helpful technical suggestions and discussions. We also thank Marilyn Morrissey, Charissa Thomas and the staff at the San Francisco VAMC Department of Nuclear Medicine for their assistance with the patient study. We also thank Rod Gullberg for assistance with the statistical analysis. This work was supported in part by the University of California Discovery Grant Program (Contract DIG06-2110-UC) and Philips Medical Systems, and in part by NIH grant number R01HL50663 and the Director, Office of Science, Office of Biological and Environmental Research, Biological Systems Science Division of the US Department of Energy under contract no DE-AC02-05CH11231.

References

Beller GA. Will cardiac positron emission tomography ultimately replace SPECT for myocardial perfusion imaging? J Nucl Cardiol. 2009; 16:841–3. [PubMed: 19885715]

Ben-Haim S, Baavour R, Haroon A, Allie R, Sitek A, Scouler A, Erlandsson K, Zia Saad Z, Breault C, Bomanji J. Assessment of myocardial perfusion reserve with dynamic myocardial perfusion SPECT. J Nucl Med. 2011; 52(Suppl 1):384.

Botvinick, EH., editor. Myocardial Perfusion Scintigraphy—Clinical Aspects (Nuclear Medicine: Cardiology). Vol. 6. Reston, VA: Society of Nuclear Medicine; 2001.

Camici PG, Rimoldi OE. The clinical value of myocardial blood flow measurement. J Nucl Med. 2009; 50:1076–87. [PubMed: 19525470]

Celler AM, Farncombe TH, Bever CA, Noll D, Maeght J, Harrop R, Lyster D. Performance of the dynamic single photon emission computed tomography (dSPECT) method for decreasing or increasing activity changes. Phys Med Biol. 2001; 45:3525–43. [PubMed: 11131182]

Coxson PG, et al. Simulation of compartmental models for kinetic data from a positron emission tomography. Comput Methods Programs Biomed. 1992; 37:205–14. [PubMed: 1511605]

Daniele S, Nappi C, Acampa W, Storto G, Pellegrino T, Ricci F, Xhoxhi E, Porcaro F, Petretta M, Cuocolo A. Incremental prognostic value of coronary flow reserve assessed with single-photon emission computed tomography. J Nucl Cardiol. 2011; 18:612–9. [PubMed: 21626091]

de Kemp RA, Trottier M, Beanlands RSB. Incremental prognostic value of coronary flow reserve assessed with single-photon emission computed tomography. J Nucl Cardiol. 2011; 18:541–3. [PubMed: 21671147]

Farncombe T, Noll D, Maeght J, Harrop R. Dynamic SPECT imaging using a single camera rotation (dSPECT). IEEE Trans Nucl Sci. 1999; 46:1055–61.

Feng B, Pretorius PH, Farncombe TH, Dahlberg ST, Narayanan MV, Wernick MN, Celler AM, Leppo JA, King MA. Simultaneous assessment of cardiac perfusion and function using 5-dimensional imaging with Tc-99m teboroxime. J Nucl Cardiol. 2006; 13:354–61. [PubMed: 16750780]

Gould KL. Does coronary flow trump coronary anatomy? JACC Cardiovasc Imaging. 2009; 2:1009–23. [PubMed: 19679290]

Gullberg GT, Di Bella EV, Sinusas AJ. Estimation of coronary flow reserve: can SPECT compete with other modalities? J Nucl Cardiol. 2001; 8:620–5. [PubMed: 11593228]

Gullberg GT, Reutter BW, Sitek A, Maltz J, Budinger TF. Dynamic single photon emission computed tomography—basic principles and cardiac applications. Phys Med Biol. 2010; 55:R111–91. [PubMed: 20858925]

Hendel RC, Cerqueira M, Douglas PS, Caruth KC, Allen JM, Jensen NC, Pan W, Brindis R, Wolk M. A multicenter assessment of the use of single-photon emission computed tomography perfusion imaging with appropriateness criteria. J Am Coll Cardiol. 2010; 55:156–62. [PubMed: 20117384]

Humphries, T. PhD thesis. Department of Mathematics, Simon Fraser University; 2011. Temporal regularization and artifact correction in single slow-rotation dynamic SPECT.

Iida H, Eberl S. Quantitative assessment of regional myocardial blood flow with thallium-201 and SPECT. J Nucl Cardiol. 1998; 5:313–31. [PubMed: 9669586]

Iida H, Eberl S, Kim K-M, Tamura Y, Ono Y, Nakazawa M, Sohlberg A, Zeniya T, Hayashi T, Watabe H. Absolute quantitation of myocardial blood flow with ^{201}Tl and dynamic SPECT in canine: optimization and validation of kinetic modeling. Eur J Nucl Med Mol Imaging. 2008; 35:896–905. [PubMed: 18202845]

Iida H, et al. Use of the left ventricular time-activity curve as a noninvasive input function in dynamic oxygen-15-water positron emission tomography. J Nucl Med. 1992; 33:1669–77. [PubMed: 1517842]

Klein R, Beanlands RS, deKemp RA. Quantification of myocardial blood flow and flow reserve: technical aspects. J Nucl Cardiol. 2010; 17:555–70. [PubMed: 20596841]

Lortie M, Beanlands RSB, Yoshinaga K, Klein R, DaSilva JN, deKemp RA. Quantification of myocardial blood flow with ^{82}Rb dynamic PET imaging. Eur J Nucl Med Mol Imaging. 2007; 34:1765–74. [PubMed: 17619189]

Murthy VL, Naya M, Foster CR, Hainer J, Gaber M, Di Carli G, Blankstein R, Dorbala S, Sitek A, Pencina MJ, Di Carli MF. Improved cardiac risk assessment with noninvasive measures of coronary flow reserve. Circulation. 2011; 124:2215–24. [PubMed: 22007073]

Patton JA, Slomka PJ, Germano G, Berman DS. Recent technologic advances in nuclear cardiology. J Nucl Cardiol. 2007; 14:501–13. [PubMed: 17679058]

Reutter BW, Gullberg GT, Huesman RH. Direct least-squares estimation of spatiotemporal distributions from dynamic SPECT projections using a spatial segmentation and temporal B-splines. IEEE Trans Med Imaging. 2000; 19:434–50. [PubMed: 11021687]

Reutter BW, Gullberg GT, Huesman RH. Effects of temporal modeling on the statistical uncertainty of spatiotemporal distributions estimated directly from dynamic cone-beam SPECT projections. Phys Med Biol. 2002; 47:2673–83. [PubMed: 12200931]

Reutter BW, Gullberg GT, Huesman RH. Accuracy and precision of compartmental model parameters obtained from directly estimated dynamic SPECT time–activity curves. IEEE Trans Nucl Sci. 2004; 51:170–6.

Reutter, BW.; Oh, S.; Gullberg, GT.; Huesman, RH. Improved quantitation of dynamic SPECT via fully 4-D joint estimation of compartmental models and blood input function directly from projections. Conf. Record of the. 2005. IEEE Nuclear Science Symp. and Medical Imaging Conf; Puerto Rico. 23–29 October 2005; 2005. p. 2337-41.

Ross SG, Welch A, Gullberg GT, Huesman RH. An investigation into the effect of input function shape and image acquisition interval on estimates of washin for dynamic cardiac SPECT. Phys Med Biol. 1997; 42:2193–213. [PubMed: 9394407]

Sitek A, Gullberg GT, Di Bella EVR, Celler A. Reconstruction of dynamic renal tomographic data acquired by slow rotation. J Nucl Med. 2001; 42:1704–12. [PubMed: 11696643]

Sitek A, Reutter BW, Huesman RH, Gullberg GT. Method of generating multiple sets of experimental phantom data. J Nucl Med. 2006; 47:1187–92. [PubMed: 16818954]

Sugihara H, Yonekura Y, Kataoka K, Fukai D, Kitamura N, Taniguchi Y. Estimation of coronary flow reserve with the use of dynamic planar and SPECT images of Tc-99m tetrofosmin. J Nucl Cardiol. 2001; 8:575–9. [PubMed: 11593222]

Tang HR, et al. Neuroblastoma imaging using a combined CT scanner-scintillation camera and ^{131}I-MIBG. J Nucl Med. 2001; 42:237–47. [PubMed: 11216522]

Yoshida K, Mullani N, Gould KL. Coronary flow and flow reserve by PET simplified for clinical applications using rubidium-82 or nitrogen-13-ammonia. J Nucl Med. 1996; 37:1701–12. [PubMed: 8862316]

Winant C, Aparici CM, Bacharach S, Sitek A, Seo Y, Gullberg GT. Measurement of the arterial input function with dynamic SPECT/CT in humans. J Nucl Med. 2009a; 50(Suppl 2):1420.

Winant, CD.; Zelnik, YR.; Reutter, BW.; Sitek, A.; Bacharach, SL.; Gullberg, GT.; Aparici, CM. Analysis of dynamic SPECT/CT measurements of the arterial input function in human subjects. Conf. Record of the. 2009. IEEE Nuclear Science Symp. and Medical Imaging Conf; Orlando, FL. 25–31 October 2009; 2009b. p. 3404-8.

Zar, J. Biostatistical Analysis. 4. Upper Saddle River, NJ: Prentice-Hall; 1999.

Zeng GL, Gullberg GT, Tsui BMW, Terry JA. Three-dimensional iterative reconstruction algorithms with attenuation and geometric point response correction. IEEE Trans Nucl Sci. 1991; 38:693–702.

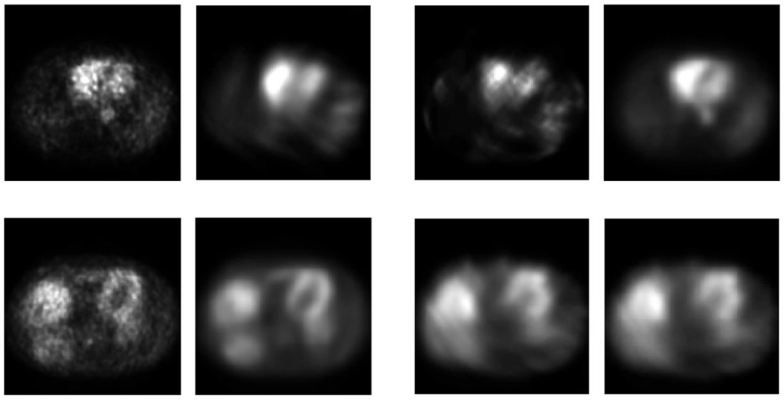

Figure 1.
Comparison of ^{94}Tc-MIBI PET (columns 1 and 2) with ^{99m}Tc-MIBI SPECT/P (columns 3 and 4). All images are of the same slice from patient 1 using an infusion time of 1 min. The top row is an early time blood pool image (weighted sum of first 60 s). The bottom row is a late-summed time image (270–420 s). Column 1: reconstructed original PET data. Column 2: same PET image as in 1, but smoothed to similar resolution (14 mm) as seen with SPECT. Column 3: 3D reconstruction of SPECT/P. Column 4: 4D reconstruction of SPECT/P data. Attenuation, collimator blurring and noise were included in the simulated SPECT/P projections.

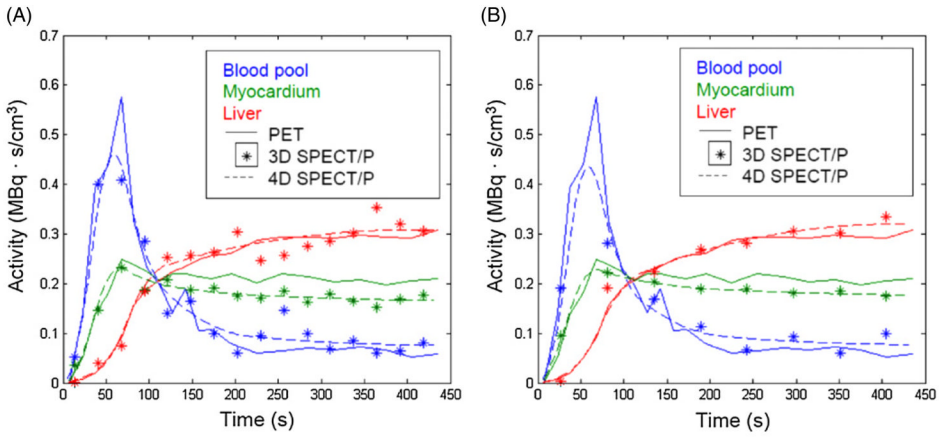

Figure 2.

Comparison of TACs derived from ^{94}Tc-MIBI dynamic PET data (patient 1) with an infusion time of 1 min and from SPECT/P projections for 27 s (A) and 54 s (B) rotations, using both 3D ML-EM (rotation-by-rotation) and 4D B-spline ML-EM reconstructions. Attenuation, collimation and realistic noise were modeled in the SPECT/P projections. Both reconstruction methods for these data incorporated attenuation correction and correction for blurring from geometric properties of the collimator. TACs from regions drawn in the LV/LA blood pool (blue), the myocardium (green) and the liver (red) are plotted from the 3D ML-EM reconstruction (asterisks) and from the 4D ML-EM reconstruction (dashed lines) for respective rotational samplings of 27 s (A) and 54 s (B) against input TACs from the original dynamic PET data (solid lines). Note that the same original dynamic PET input curves are shown for comparison in each panel.

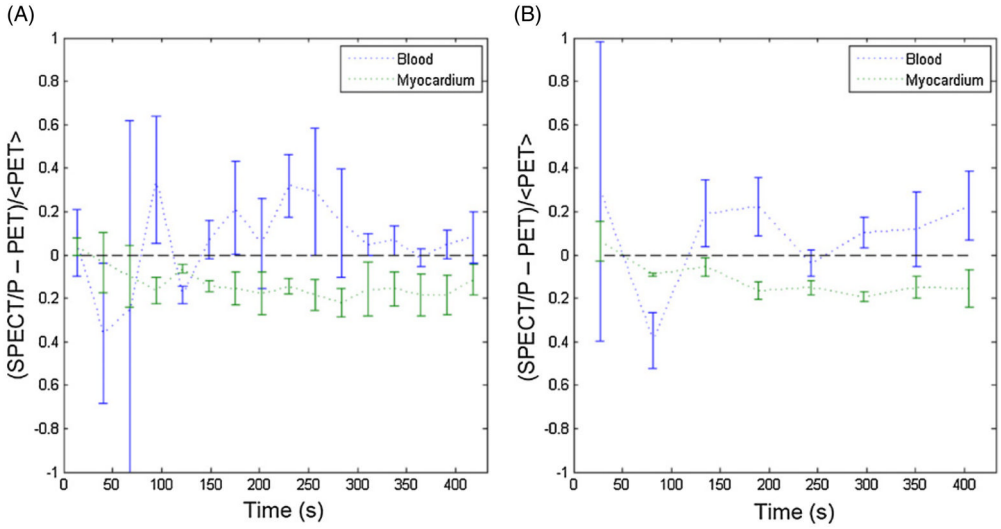

Figure 3.

Residual difference curves between PET and 3D ML-EM SPECT/P TACs, averaged for all three PET patients. Part A shows residuals for the 27 s rotation data. Part B shows residuals for the 54 s rotation data. In both panels, the difference between the blood curves is shown in blue and the difference between the myocardium tissue curves is shown in green. The error bars at each time point represent the standard deviation about the mean over all three patients. The difference curves are normalized by the mean PET activity over each dynamic study.

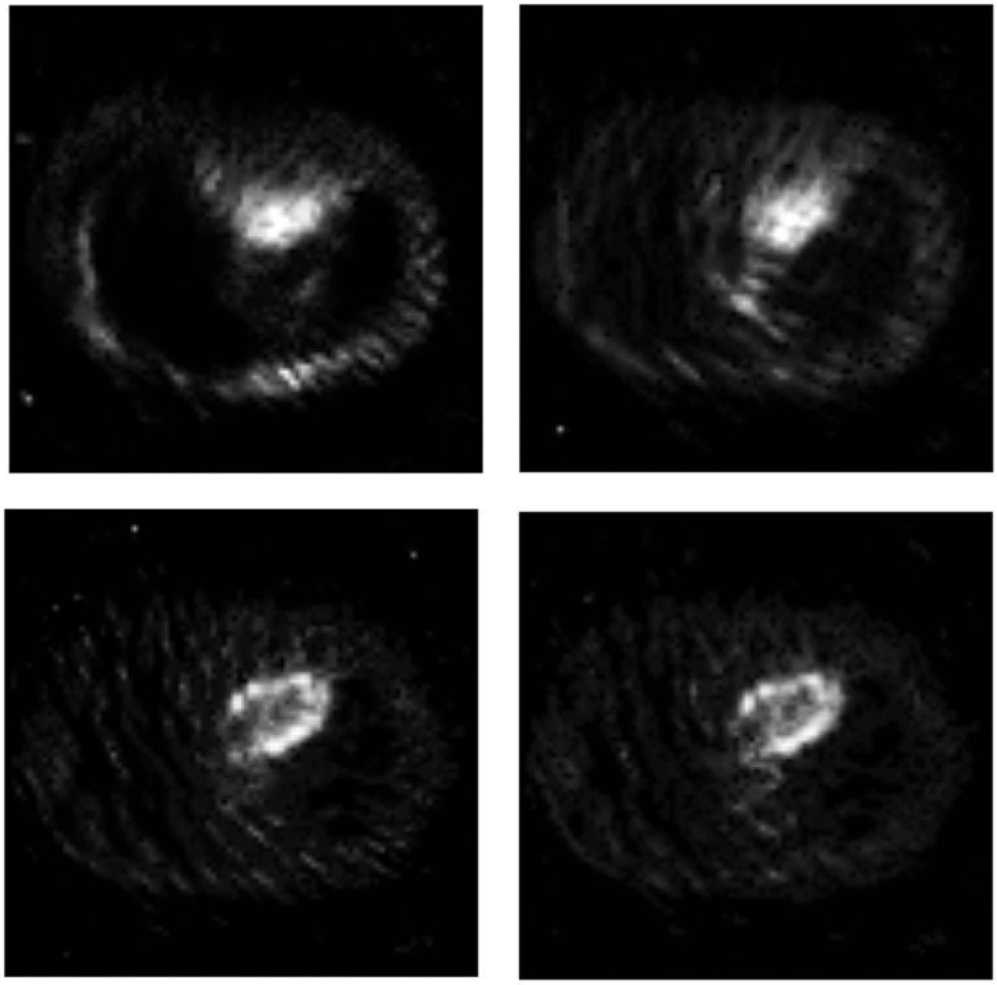

Figure 4.
Side-by-side comparisons of the 54 s rotation SPECT/D transaxial-slice images of the anthropomorphic torso phantom with cardiac insert, at early and late times. The top-row images are of the blood pool at early times (weighted sum 0–60 s) and the bottom-row images are of the myocardium (weighted sum 378–432 s). In each row, the image in the left column was reconstructed with 3D ML-EM and the image in the right column was reconstructed with 4D ML-EM.

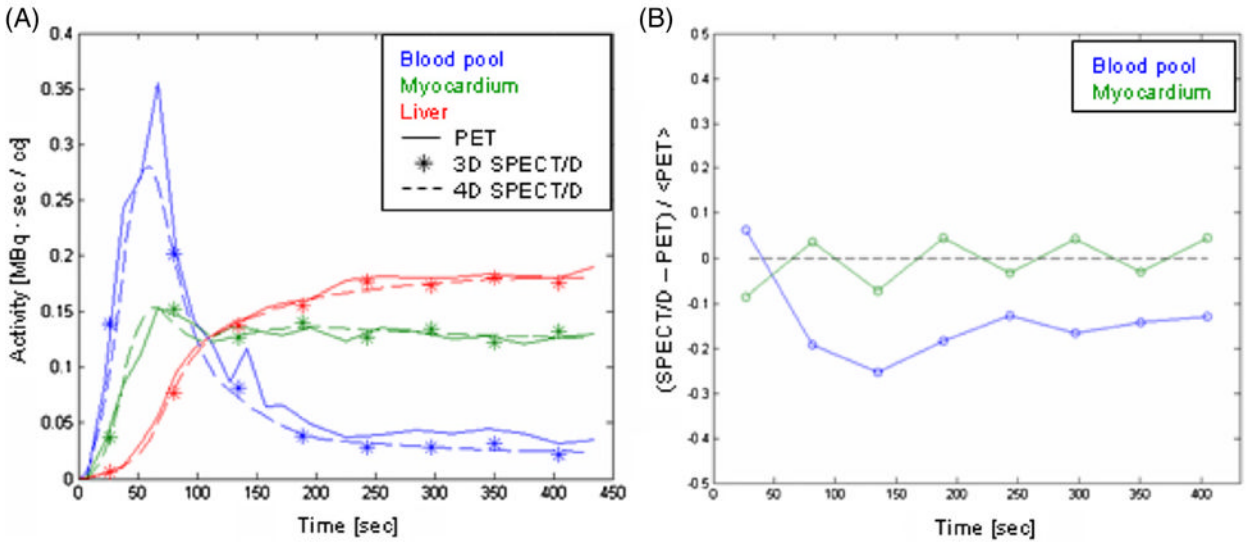

Figure 5.

(A) Comparison of TACs derived both from ^{94}Tc-MIBI dynamic PET data (patient 1) and from the anthropomorphic Jaszczak phantom SPECT/D data (54 s rotations using same ^{94}Tc-MIBI PET inputs), using 3D rotation-by-rotation ML-EM and 4D B-spline ML-EM reconstructions. TACs from regions drawn in the LV/LA blood pool (blue), the myocardium (green) and the liver (red) are plotted from the 3D ML-EM reconstruction (asterisks) and from the 4D ML-EM reconstruction (dashed lines) against input TACs from the original dynamic PET data (solid lines). (B) Difference curves between PET and 3D ML-EM SPECT/D 54 s rotation TACs. The difference between the blood pool TACs is shown in blue, and the difference between the myocardium tissue TACs is shown in green.

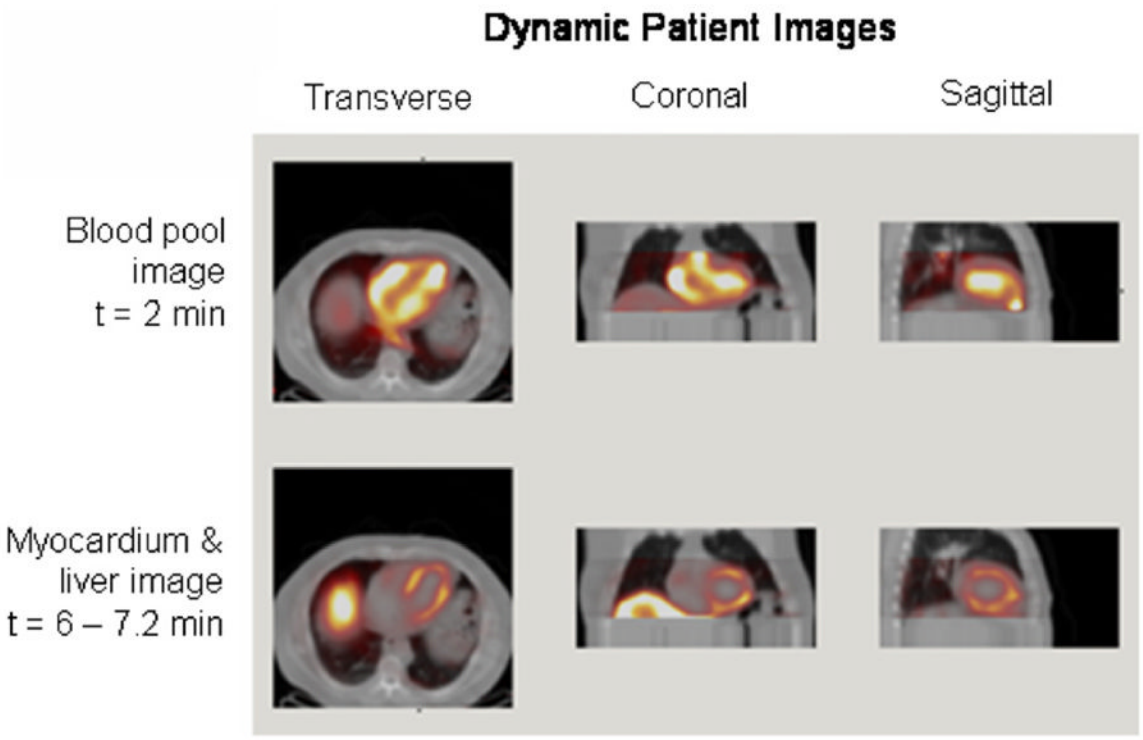

Figure 6.

Three orthogonal (from left to right, transverse, coronal and sagittal) views of the 4D ML-EM reconstructed tracer distribution (red temperature color-scale), overlaid on the CT attenuation map, of a male patient (246 pounds), imaged with a Philips Precedence™ SPECT/CT while given a 2 min constant 629 MBq (17 mCi) infusion of ^{99m}Tc-tetrofosmin. Top panel: t = 2 min after beginning of imaging. Bottom panel: t = 6–7.2 min after beginning of imaging.

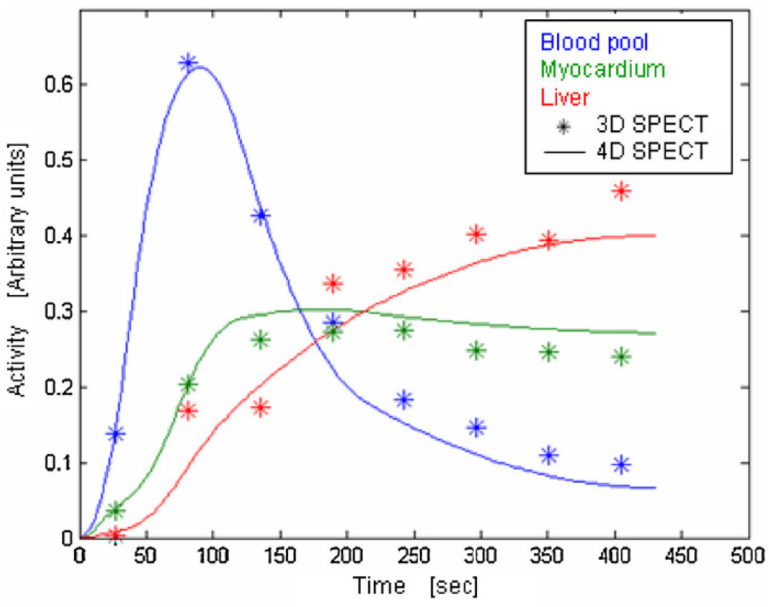

Figure 7.

Comparison of 4D-reconstruction (solid) and static-reconstruction (3D ML-EM) (asterisks) TACs for the blood pool (blue), myocardium (green) and liver (red) of a male patient (246 pounds), imaged with a Philips Precedence™ SPECT/CT who was given a 2 min infusion of 629 MBq (17 mCi) of ^{99m}Tc-tetrofosmin. The units of activity are arbitrary.

Table 1

Comparison of single-compartment model uptake kinetic parameters, K_1, and 1σ (unweighted) estimated errors from dynamic PET and from SPECT/P.

Data	Seconds/rotation	Reconstruction method	K_1 (patient 1) (min^{-1})	Bias	K_1 (patient 2) (min^{-1})	Bias	K_1 (patient 3) (min^{-1})	Bias
PET	NA	OSEM	0.425 ± 0.010		0.278 ± 0.010		0.391 ± 0.012	
SPECT/P	54	4D ML-EM	0.526 ± 0.005	0.101**	0.220 ± 0.002	−0.058**	0.401 ± 0.003	0.010
SPECT/P	54	3D ML-EM	0.462 ± 0.036	0.037**	0.203 ± 0.053	−0.075**	0.318 ± 0.033	−0.073**
SPECT/P	27	4D ML-EM	0.430 ± 0.001	0.005**	0.156 ± 0.001	−0.122**	0.354 ± 0.008	−0.037**
SPECT/P	27	3D ML-EM	0.407 ± 0.029	−0.018*	0.141 ± 0.024	−0.137**	0.327 ± 0.025	−0.064**

* The absolute bias is statistically significant at the 0.05 level employing Dunnett's test (Zar 1999).

** The absolute bias is statistically significant at the 0.01 level employing Dunnett's test.